Journal of Merchant Ship Wind Energy

Translation of B. Wagner's Angled towing tests for a sailing vessel hull with and without bar keel and for the "Mariner" (Schrägschleppversuche für einen Seglerrumpf mit und ohne Balkenkiel und für den "Mariner")

Lubomir A. Ribarov, Ph.D., Department of Marine Engineering, U.S. Merchant Marine Academy, Kings Point, NY, May 2022 ribarovl@usmma.edu

Originally published in German by Institute for Shipbuilding of the University of Hamburg, Report No. 186, 1968, Schrägschleppversuche für einen Seglerrumpf mit und ohne Balkenkiel und für den "Mariner".

ABSTRACT

Results are presented from ship model towing tank tests, conducted at a variety of leeway angles. Two models are tested, and the influence of a bar keel, hull shape, rudder angle, rudder position on hull force and yaw moment coefficients is determined. Test results were analyzed using current as well as novel techniques.

Organization:

1. Introduction

On a maneuvering ship, balance of moments and forces must be maintained at all times. For this reason, numerous theoretical and experimental efforts have been made in order to determine the hydrodynamic forces and moments of maneuvering ships – i.e., mostly sailing with a drift angle traveling on a curved path. The tests are generally performed in a circular channel, where the curve radius (and thus the circular curvature) and drift angle can be set and the forces and moments determined as a function of drift angle, path curvature and velocity. Such experiments are carried out with or without a running propeller. The angled towing test is practical in the extreme case when the path curvature is zero. This test was conducted in a normal ("straight") towing tank.

Of interest are the following: the lateral force Y (force component orthogonal to the ship's longitudinal direction), the yaw moment N, the center of pressure position of the underwater force, and the increase in resistance (more precisely, the additional longitudinal force in the event of drift (leeway angle). Angled towing test results are always significant, if one considers the state of equilibrium of the ship in translation when external forces are applied, i.e. with wind (extreme in the case of a sailing ship), lateral hawser pull, etc.

The reason for the investigation described here is the testing of a calculation method developed by the IfS[1] to predict the speed of sailing ships. For these calculations, the resistance increase caused by drift (leeway angle or angled orientation of the hull) plays a big role. A force opposing the side component of the air (wind) force must constantly be generated by the hull of the sailing vessel, which occurs due to yawing of the hull, and results in an increase in resistance [1]. The same applies, of course, for every ship exposed to side winds. In [2] it was shown that this additional force in the longitudinal direction is also experienced by motor ships and is usually

[1] IfS = Institut für Schiffbau (Institute for Shipbuilding) – where B. Wagner worked at the TUHH – translator remark

L. A. Ribarov, Translation of B. Wagner's Angled towing tests for a sailing vessel hull with and without bar keel and for the "Mariner" (Schrägschleppversuche für einen Seglerrumpf mit und ohne Balkenkiel und für den "Mariner"), Journal of Merchant Ship Wind Energy, May 2022, www.jmwe.org

considered solely as “wind resistance”. One of the models used in this work is a reproduction of the 4-masted “Pamir”[2] . The model of the “Mariner” was available from the IfS[3]. The tests were planned to provide useful data for future ship designers, i.e. the creation of documents on the hydrodynamic forces and moments on the ship’s hull with angled flow to calculate the speed of sailing ships. These are of general interest for the investigation of maneuvering properties of ships. Therefore, particular importance was attached to the analysis of the test results.

2. Tasks

With the selected two models, i.e. the sailing ship and the “Mariner”, a bigger systematic test program could not be conducted, as would be desirable, since relatively few results of angled towing tests have been published to date.

The described tests had the goal to determine the forces and moments on the underwater hull at small leeway angles (drift angle $\beta \leq 20°$). Of particular interest were here:

Influence of a bar keel
Influence of hull form
Influence of aspect ratios of the underwater hulls ($\Lambda = \frac{2 \cdot T}{L_{pp}}$)
Influence of the rudder location and
Influence of Froude number on the forces and moments

It could not be expected that the test results would be sufficient to generally calculate these influences with sufficient accuracy.

[2] Translator’s note: the “Pamir” (together with sister ship “Passat”) rounded cape Horn on 10 July 1949; the last time a cargo-carrying sailing vessel would do so. Pamir sank in 1957 during hurricane Carrie.
https://museum.wales/collections/online/object/6bdfbe6a-8fd2-36f7-b871-7f9cdd01dad0/PAMIR-full-hull-model-of-sailing-ship/

[3] The Mariner ship was developed by the U.S. Maritime Administration (MARAD) after WWII and became a successful ship design adopted by shipping companies. The Mariner was one of a handful of similar ships chosen for development of Series 60 hull forms.
L. A. Ribarov, Translation of B. Wagner’s Angled towing tests for a sailing vessel hull with and without bar keel and for the “Mariner” (Schrägschleppversuche für einen Seglerrumpf mit und ohne Balkenkiel und für den “Mariner”), Journal of Merchant Ship Wind Energy, May 2022, www.jmwe.org

3. Description of the Models

The main measurements as well as the ratio values of interest for the models can be found in the following overview:

	Four-mast barque (lines after [3])	"Mariner" (lines after [4])	
Scale	1:48	1:80	
L_{pp}	2.00	2.012	m
B	0.298	0.290	m
T_{MAX}	0.150	0.103/0.123	m
T	0.142		
V	0.0584	0.036/0.044	m^3
δ	0.69	0.60/0.62	
$\Lambda = \frac{2 \cdot T}{L_{pp}}$	0.142/0.150	0.102/0.122	
L/B	6.71	6.95	
β	0.907	0.981	

The lines of the models are shown in Fig. 1 and 2.
The sailing vessel hull was made of wood and coated (lacquered), keel and bar stern (metal) were removable. The flat rudder could be fixed at any desired angle of attack.

The "Mariner" model was made out of GFK[4]*. It had an adjustable balanced rudder made out of wood. A 1.5 mm Perlon wire on frame 19 was used as a turbulence generator. Resistance values were corrected to compensate for the added drag of the wire.

[4] * Glasfaserverstärkter Kunststoff (FRP/GRP - Fiberglass Reinforced Plastic)

Fig. 1 Four-mast barque model

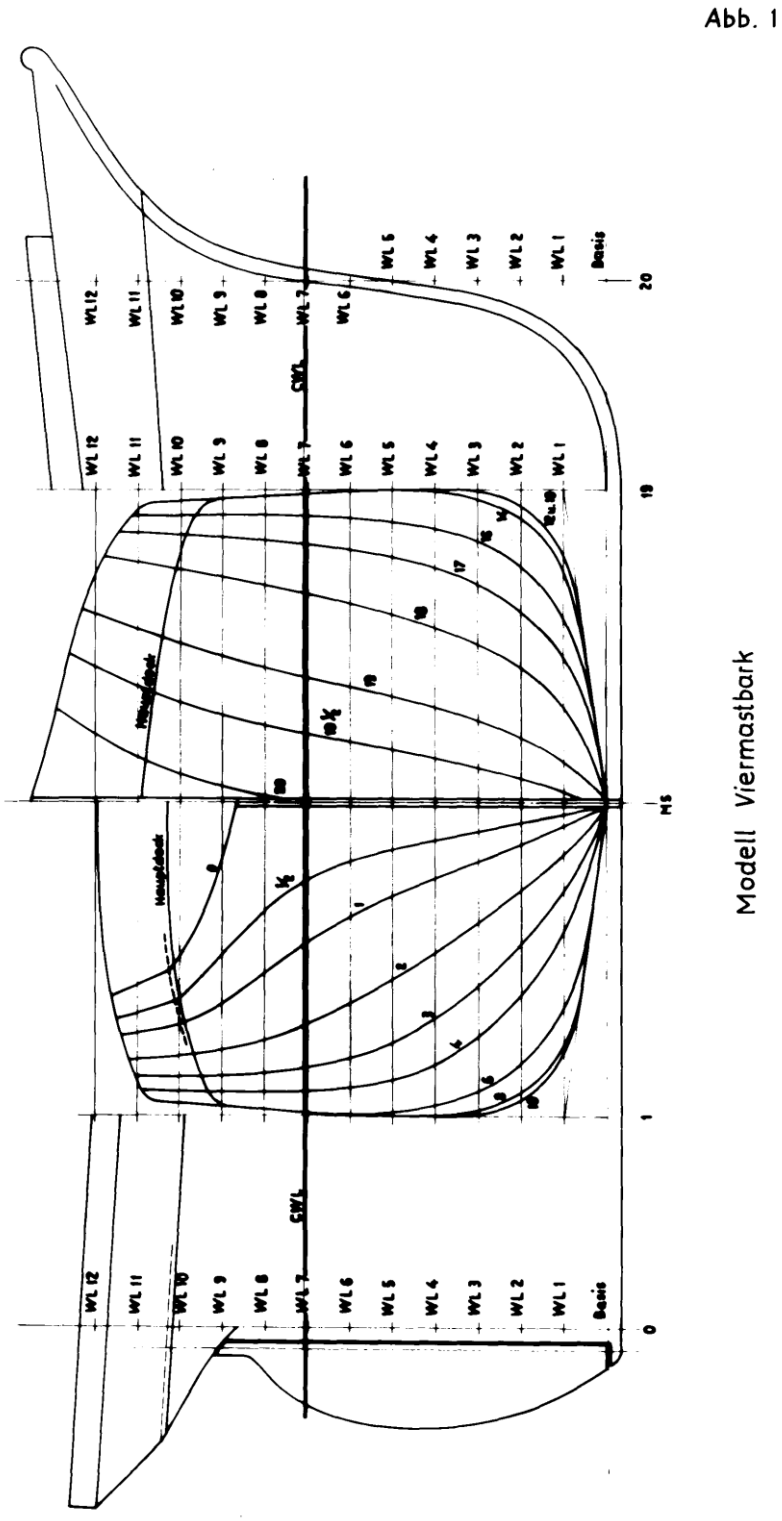

Fig. 2 Mariner model

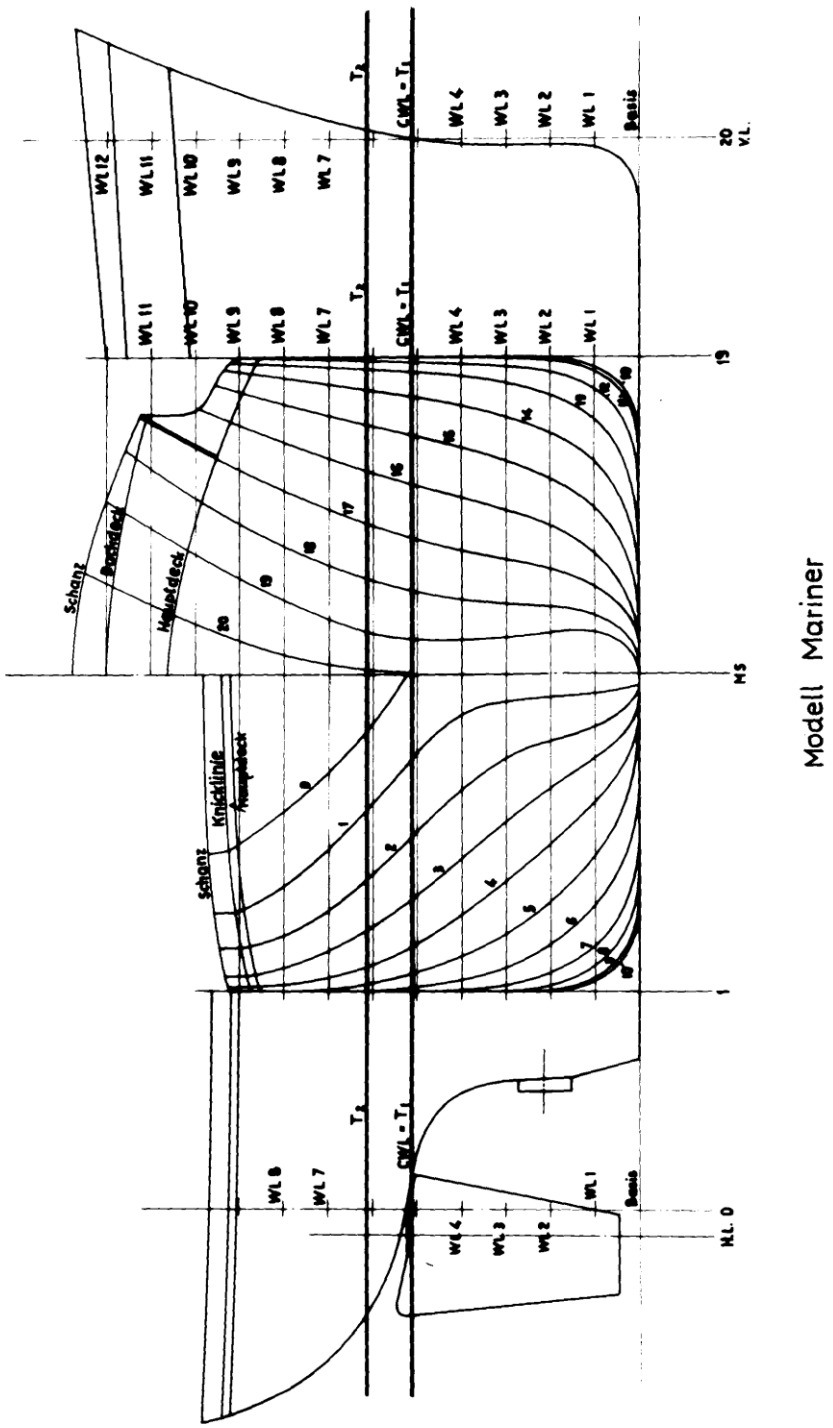

4. Test setup and implementation (execution) of tests

The tests were conducted in the small tank of the HSVA[5] (length 80 m, width 5 m, depth 3m). The electric 3-component spring joint scale of the IfS with 3 sensors of 10 kp measuring range was used[6].

The model was connected to the three-component scale via a special device that allowed free hoisting, trimming and diving[7] (cf. Fig. 3). Free hoisting and trimming were achieved with a coupling immediately at the attachment point of the model of $L_{pp}/2$ in the waterline. The connection between the link and the scale was built from a hardened steel pipe that ran parallel in a ball bearing bushing and allowed unobstructed diving.

With the turning device of the scale any desired drift angle of the model could be set. In order to eliminate the influence of the heel on the measurement results, the heel was set to zero during the travel before the measurement by shifting the weight to the side. These methods yielded – albeit with unsatisfactory accuracy – also the rolling moment. In the described tests it was only important to keep the heeling as small as possible. For an exact measurement of the rolling moment, the measurement of the heeling had to be improved (e.g. spirit level instead of pendulum wire).

The measurement device itself was of worse quality: there were frequent shocks, which led to stronger vibrations of the towing truck (cart) and to fluctuations in the measured values. For this reason, low-pass filters were connected in front of the carrier frequency measuring amplifiers feeding the strain gage sensors. The measured values were written on a quiescent track section using an oscilloscope, namely two resistance components and one lateral force component. For the determination of the speed of the towing cart, a way scriber on a synchronous drum was used.

[5] HSVA = Hamburgische Schiffbau-Versuchsanstalt GmbH (Hamburg Ship Model Research Basin) – translator remark
[6] A kp-index is a scale used to characterize the magnitude of geomagnetic disturbances (translator remark)
[7] "diving" here may be understood in the context of pushing the model into the water at different drafts (translator remark)

Fig. 3 Model mount: equipment for free submerging, heeling and trimming (sketch approx. 1:4)

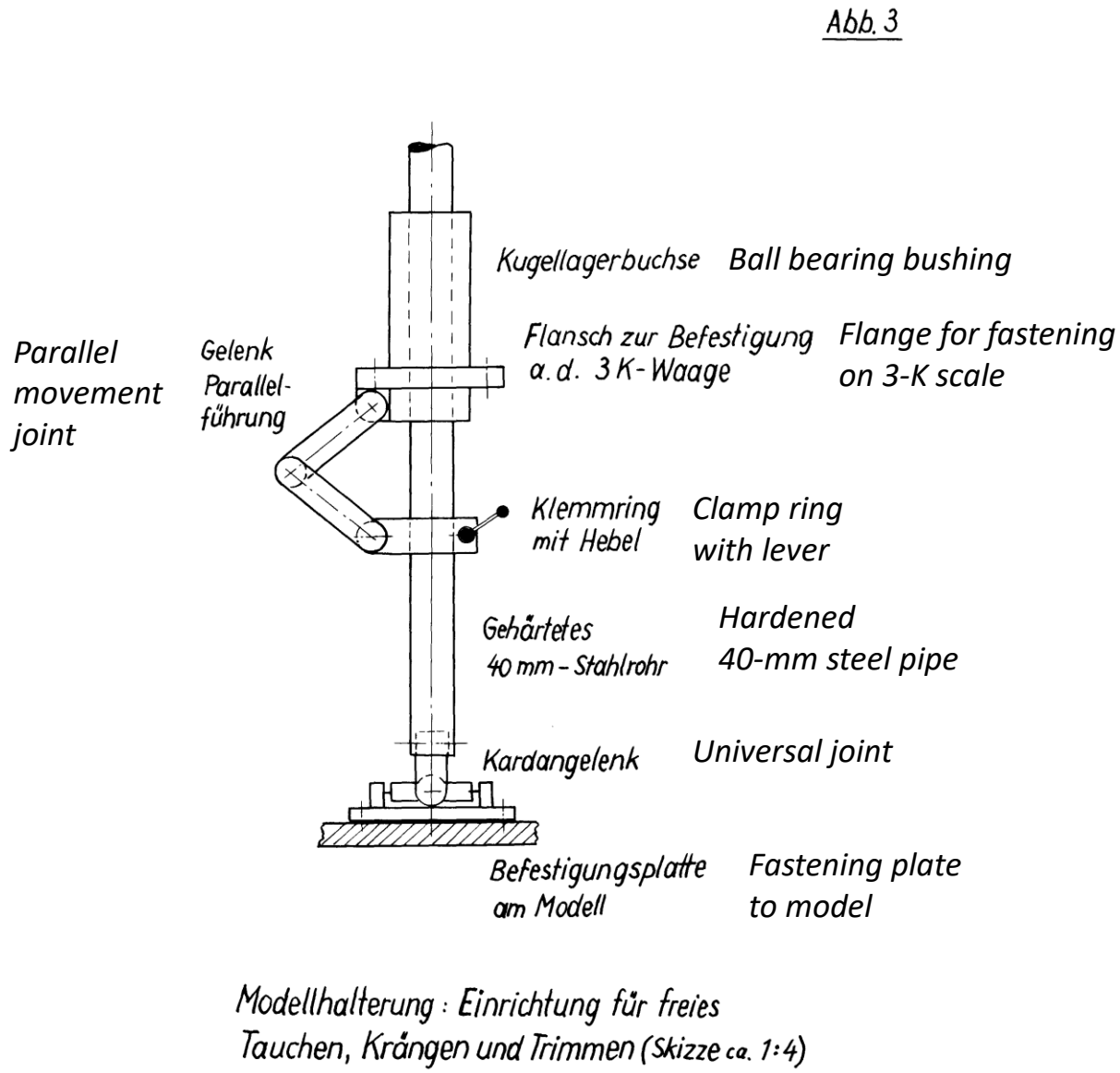

Overview of the Tests

	No. Nr.	Model Modell	Remark Bemerkung	V [m/s]	F_n	Drift angle Driftwinkel β	δ_R	Fig. Abb.	Tab.
4-mast barque with keel	1	Viermastb.	mit Kiel	0,692	0,155	0,2,5,7,10,12,15,20	0°	4	1.1
	2	"	"	0,897	0,203	"	0°	4	1.2
	3	"	"	0,690	0,155	0,2,5,7,10,12,15	10°	5	2
	4	"	"	0,684	0,155	0,2,5,7,10,12,13,15	20°	5	3.1
	5	"	"	0,890	0,203	0,2,5,7,10,12,15	20°	6	3.2
without keel	6	"	ohne Kiel	0,678	0,155	0,2,5,7,10,12,15,20	0°	7	4.1
	7	"	"	0,895	0,203	"	0°	7	4.2
	8	"Mariner"	T_1=0,103 m	0,690	0,155	0,2,5,7,10,12,15,20	0°	8	5.1
	9	"	"	0,899	0,203	"	0°	8	5.2
	10	"	T_2=0,123 m	0,684	0,155	"	0°	9	6.1
	11	"	"	0,900	0,203	"	0°	9	6.2
	12	"	"	1,232	0,279	"	0°	9	6.3

Remarks on the Evaluation Method

The average deflection from the zero position for the individual components was determined on the oscilloscope (oscillography) track (record) for a section with the smallest possible fluctuations in the measured values.
Taking into account the measuring range, the 3 force components then resulted from the calibration curves. By plotting the individual components over the drift angle, the measurement results were checked for errors and corrected if necessary.

The value of the resistance in the event of an inflow from the front was taken from special towing tests due to the greater accuracy (sailing vessel hull, see Appendix) or checked by converting other towing test results (“Mariner”).

5. Description of the measurement results

The previous overview has a description of the measurement results included in the figures and tables.

From the original measurement data-the force components (lateral force C, resistance D) and the yaw moment N were calculated and non-dimensionalized. The dimensionless coefficients were defined as follows (cf. Fig. 10):

Lateral force coefficient $c_C = \frac{C}{q \cdot L_{pp} \cdot T}$

Resistance force coefficient $c_D = \frac{D}{q \cdot L_{pp} \cdot T}$

Yaw moment coefficient $c_N = \frac{N}{q \cdot L_{pp} \cdot T}$

(editor's note: The equation for Cn above must have a typographical error since the units do not cancel. It can be shown that the formula should read:

$c_N = \frac{N}{q\, Lpp^2 T}$,

from the equation $x_f/L_{pp} = c_N/c_y$ *below.)*

The moment coefficient C_N uses Lpp/2 as reference.). C is the lift force of the hull perpendicular to the direction of motion of the ship, D is the total water drag on the ship hull ("straight-ahead" drag + drag from angled motion), opposite to the direction of motion of the ship.)

Where:

$q = \frac{\varrho}{2} \cdot v^2$ dynamic pressure of the flow speed

L_{pp}, T Length between the perpendiculars, Draft (max) (instead of lateral side faces underwater was the L_{pp} T set for simplification)

Under resistance, we recognize (distinguish) two components:

$D = D_0 + D_C$

D_0 resistance for forward motion (movement) ($\beta = 0$)

D_C resistance increase from oblique flow ("lateral force resistance"), (generally, induced resistance)

The force components in the ship's longitudinal and orthogonal directions can thus be calculated from the following equations:

$c_X = c_C \cdot \sin\beta - c_D \cdot \cos\beta$ (coefficient of the longitudinal force)

$c_Y = c_C \cdot \cos\beta + c_D \cdot \sin\beta$ (coefficient of the side force)

From the yaw moment coefficient and the side force coefficient one can obtain the center of pressure location x_F, measured from $L_{pp}/2$:

$x_F/L_{pp} = c_N/c_Y$ the location of the pressure points from the moment reference point ($L_{pp}/2$)

The distance e from the pressure point (center of pressure) to the most forward perpendicular is defined by:

$$\frac{e}{L_{pp}} = 0{,}50 - \frac{x_F}{L_{pp}}$$

The glide ratio (induced drag/lift) of the forces on the underwater hull was calculated by:

$$\epsilon_{CH} = \frac{D_C}{C} = \frac{c_{DC}}{c_C}$$

(Editor's note: Wagner does not explicitly define c_{DC} and Cc, but we can deduce that c_{DC} is a lateral force resistance coefficient (which includes induced drag and form drag) and C_c is the hull lift coefficient or hull lateral force coefficient))

Methods of Application:

One may create a "hull polar diagram" by plotting D_C (hull drag due to lateral force) with C (lift of the hull). The hull polar clearly displays the drag penalty associated with increasing the hull's lateral resistance.

Later, the glide ratio ε_{CH} will be used in the dimensionless parameter c_C/Λ (see below!).

6. Experimental Results

The experimental results are displayed in Fig. 4 [8]. The drawings contain lateral force coefficient value c_C and lateral force resistance coefficient value c_{DC} *)[9] as a function of drift angle β and the rudder angle δ_R. In addition, the hull polars $c_C = f(c_{DC})$ are shown. The results for the different models and model variants will be presented below.

Sailing vessel hull with bar keel and bar stern: Fig. 4 contains the experimental results for two Froude numbers. One sees that the influence of the Froude number on the lateral force coefficient cc is small. On the other hand, the lateral force resistance coefficient c_{DC} decreases with increasing Froude number. The induced resistance (drag) should not have changed, however only part of the lateral force resistance is induced resistance. The hull polar changes accordingly. For small β the center of pressure of the hull forces moves forward with higher Froude number. It moves backwards[10] with increasing drift angle.

---

[8] For better readability, figures have been moved from the end of the document, closer to where they are discussed.

[9] *) like yaw moment coefficient c_N and the pressure point location $\frac{e}{L_{pp}}$

[10] Towards the rear – translator's note

Fig. 4 Sailing vessel hull with bar keel

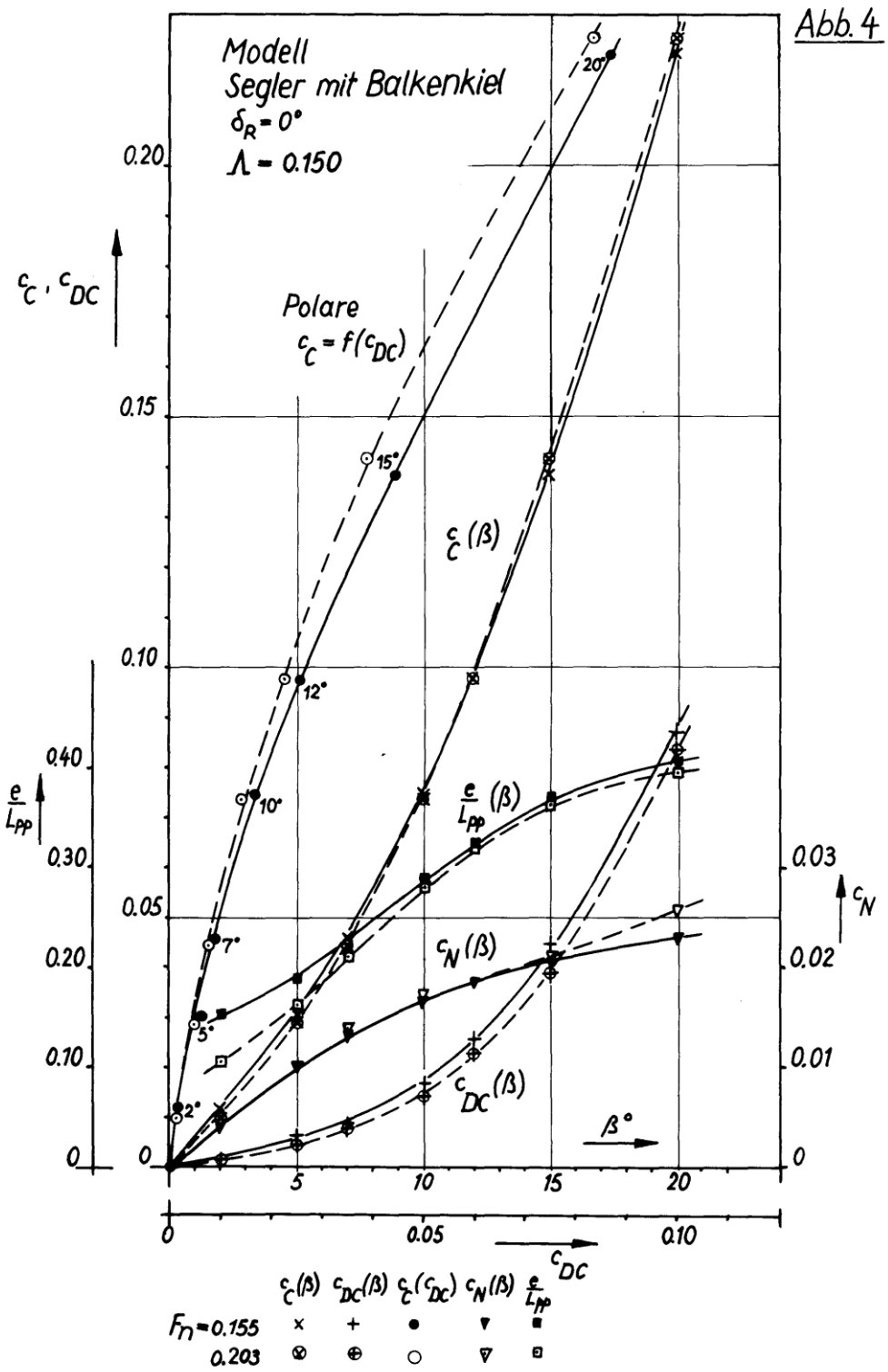

L. A. Ribarov, Translation of B. Wagner's Angled towing tests for a sailing vessel hull with and without bar keel and for the "Mariner" (Schrägschleppversuche für einen Seglerrumpf mit und ohne Balkenkiel und für den "Mariner"), Journal of Merchant Ship Wind Energy, May 2022, www.jmwe.org

Influence of the position of the rudder (Sailing vessel hull with keel). (Figs. 5 and 6):

The influence of the position of the rudder was investigated for rudder positions $\delta_R = 10°$ and 20°, but is comparatively unclear for the $\delta_R = 10°$. These influences are more recognizable for the $\delta_R = 20°$ equally for both Froude numbers: the lateral force coefficient c_C and the lateral force resistance coefficient c_{DC} are opposite $\delta_R = 0°$ throughout the range increasing with β increased. The center of pressure shifts with the rudder down – as expected – towards the rear, through which it decreases by the $L_{pp}/2$ related yaw moment coefficient

Fig. 5 Model of sailing ship with bar keel. $F_n = 0.155$.

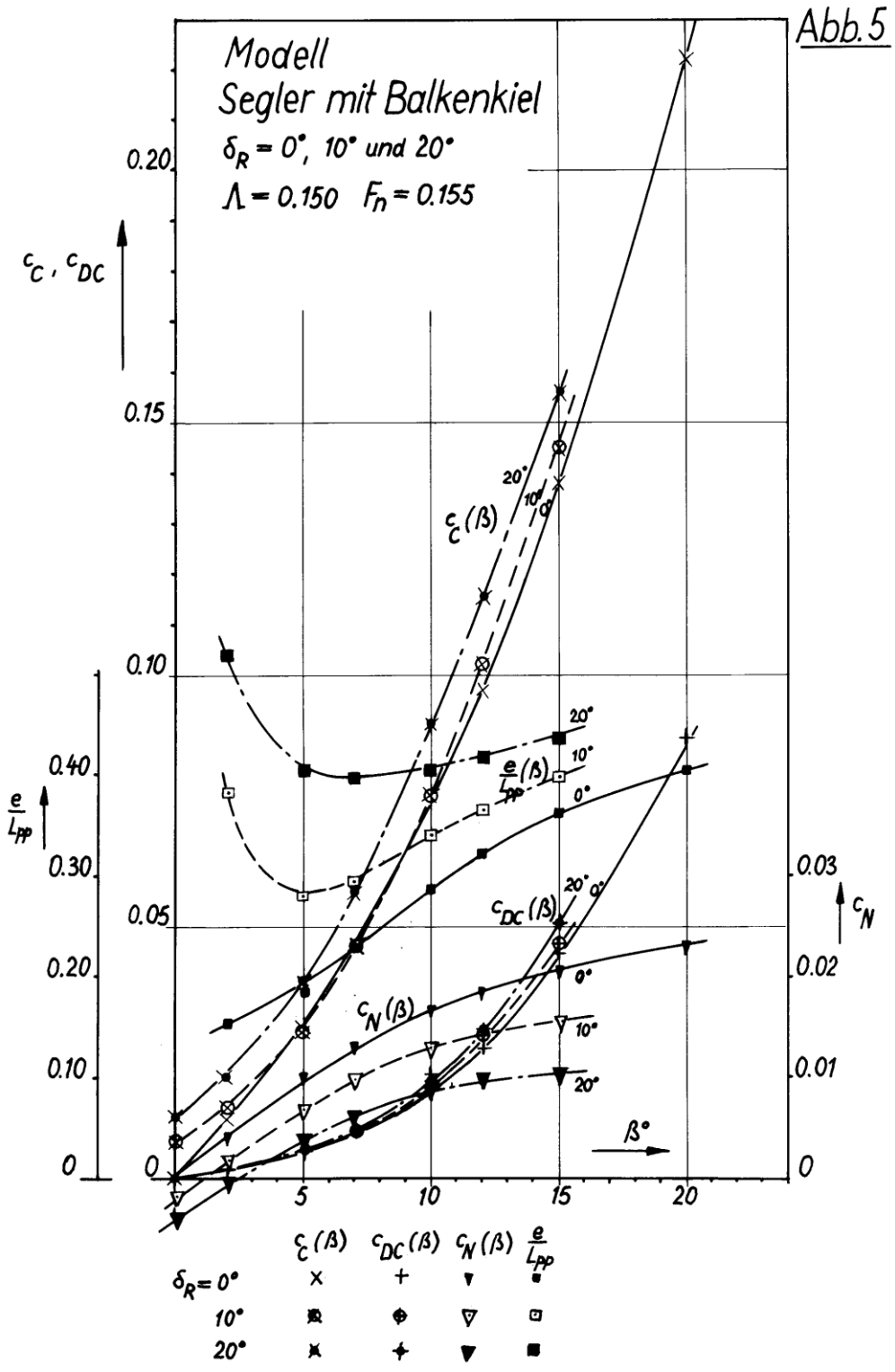

L. A. Ribarov, Translation of B. Wagner's Angled towing tests for a sailing vessel hull with and without bar keel and for the "Mariner" (Schrägschleppversuche für einen Seglerrumpf mit und ohne Balkenkiel und für den "Mariner"), Journal of Merchant Ship Wind Energy, May 2022, www.jmwe.org

Fig. 6 Model of sailing ship with bar keel. $F_n = 0.203$

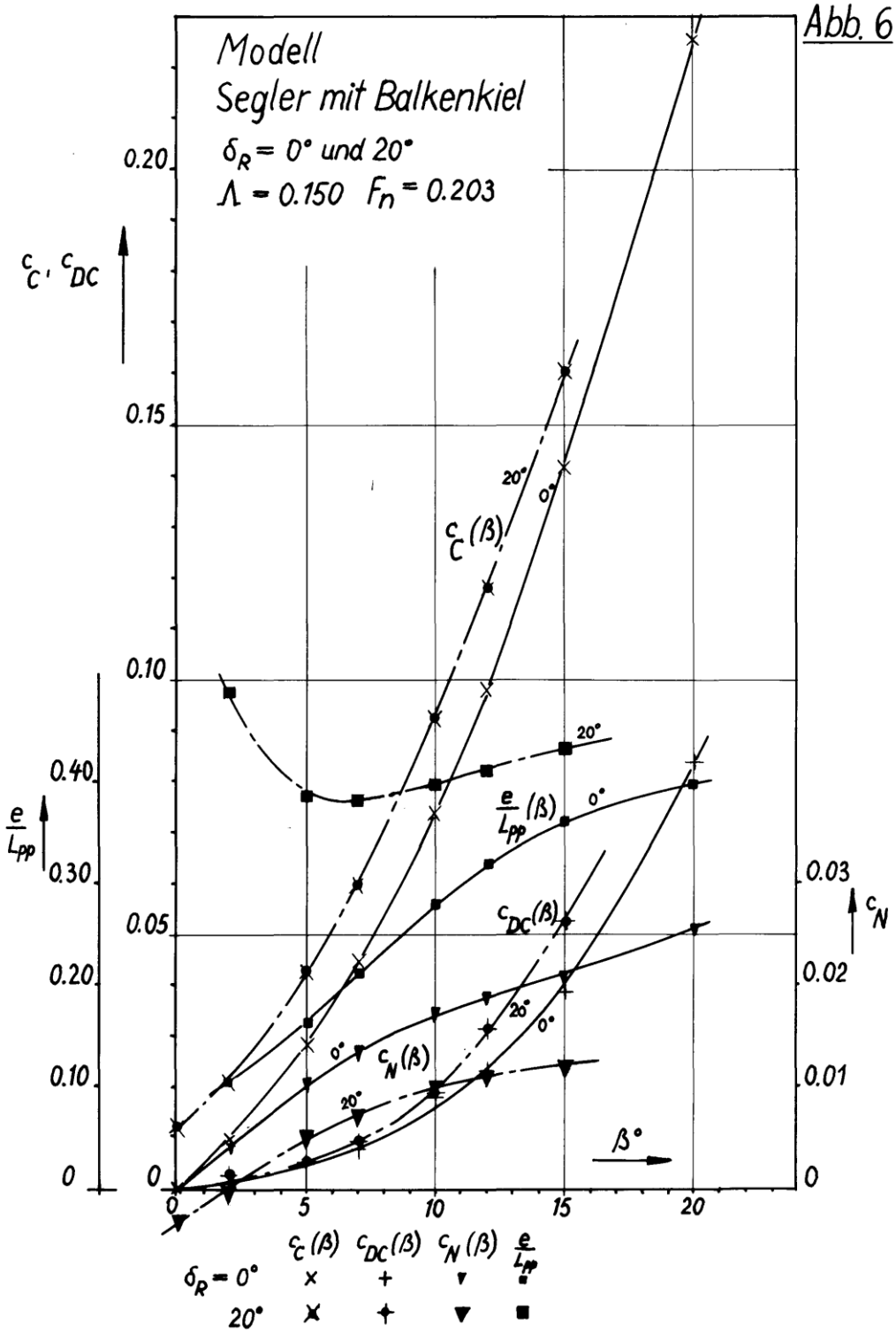

L. A. Ribarov, Translation of B. Wagner's Angled towing tests for a sailing vessel hull with and without bar keel and for the "Mariner" (Schrägschleppversuche für einen Seglerrumpf mit und ohne Balkenkiel und für den "Mariner"), Journal of Merchant Ship Wind Energy, May 2022, www.jmwe.org

Sailing vessel hull without keel:

The removal of the bar keel and bar stern decreased the yaw moment and the yaw moment resistance coefficient. Little change was observed in the location of the hull center of pressure.

Froude number dependency: at the higher Froude number again a smaller yaw moment resistance coefficient occurred. For small drift angles the lateral force coefficient is also noticeably lower. At the higher Froude number, the center of pressure lies further ahead in the entire range.
If one compares the sailing vessel hull polars with- and-without bar keel, it would seem that they are close in value in the entire range of small drift angle ($\beta < 10°$). This means that the emerging resistance increase at the generation of a distinct yaw moment with and without keel is equal, but with keel the required angle of the flow (drift angle) is smaller.

Fig. 7 Model of sailing ship without bar keel (next page)

Abb. 7

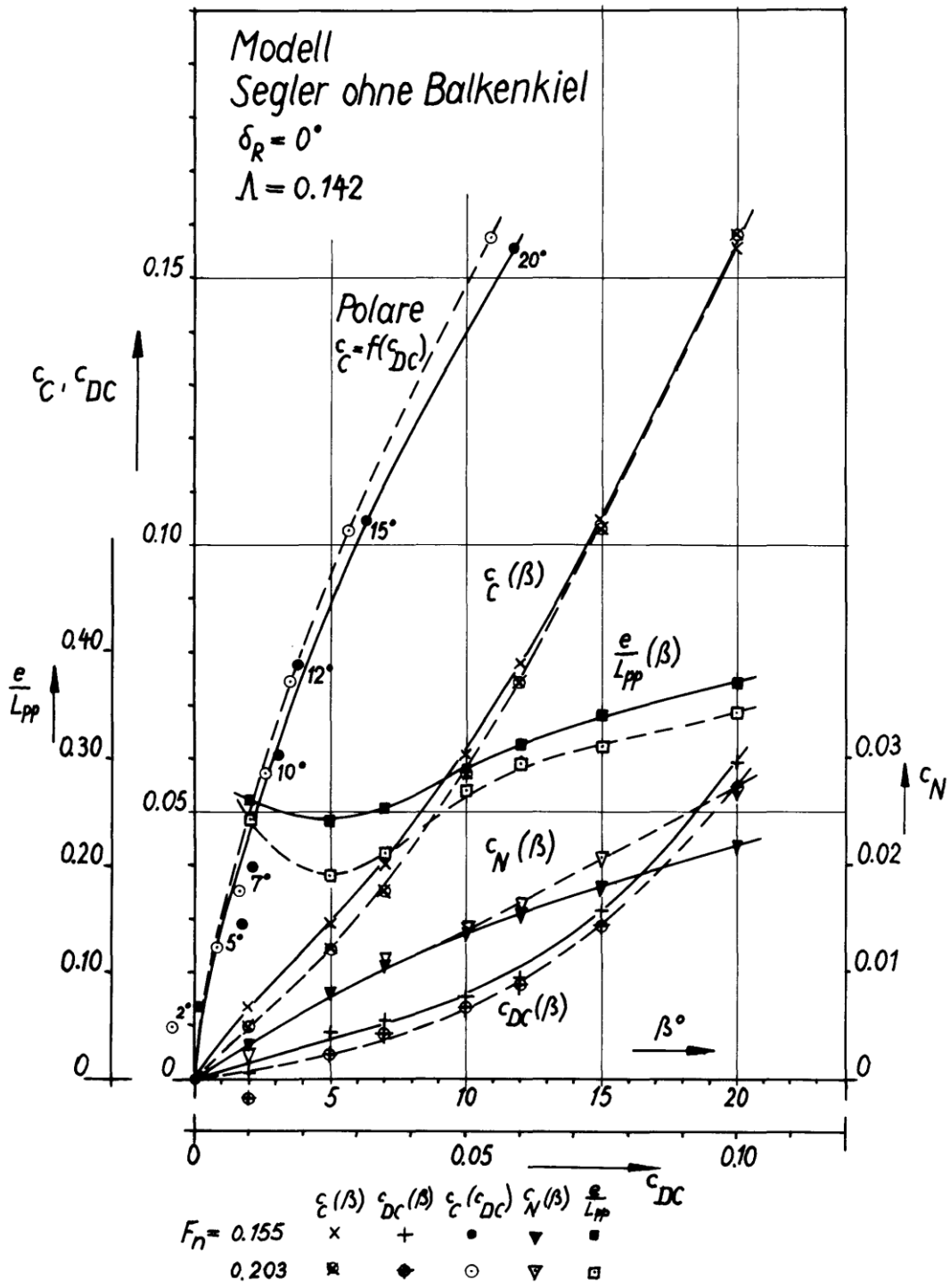

L. A. Ribarov, Translation of B. Wagner's Angled towing tests for a sailing vessel hull with and without bar keel and for the "Mariner" (Schrägschleppversuche für einen Seglerrumpf mit und ohne Balkenkiel und für den "Mariner"), Journal of Merchant Ship Wind Energy, May 2022, www.jmwe.org

Mariner at design draft:
An increase in the Froude number had resulted in a (weaker) decrease of c_C and a (stronger) increase of c_{DC} in the entire range of small drift angle. Also, it is very clear that the center of pressure moves forward with increasing Froude number.

Fig. 8 Mariner at design draft = 0.103 m.

Abb. 8

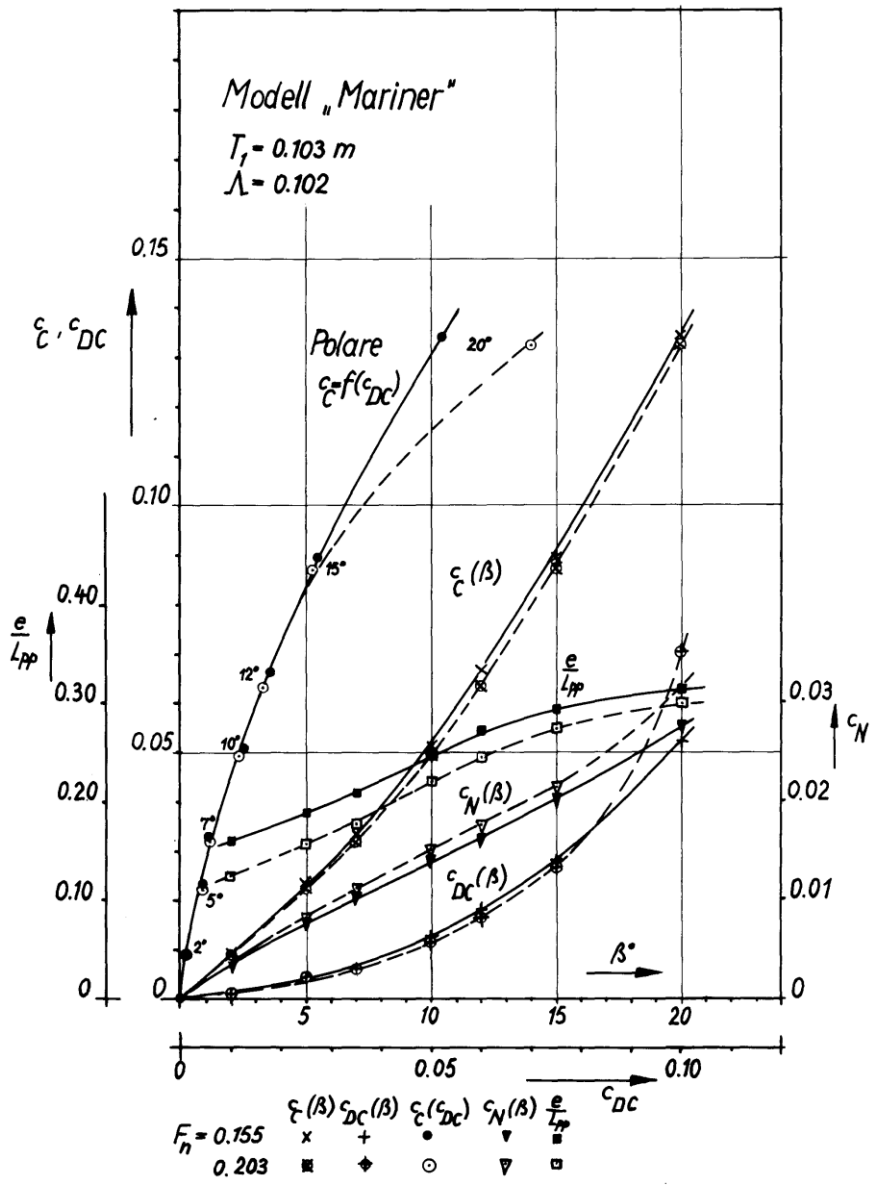

"Mariner" at bigger draft T_2:

The influence of F_n (in this case 3 F_n values were investigated) on c_C and c_{DC} is relatively large. The lateral force coefficient c_C decreased with increasing Froude number, while c_{DC} has a clear decreasing tendency. The center of pressure movement in turn is to forward with rising Froude number.
An equation with the coefficients for the smaller draft T_1 shows a clear increase in the lateral force coefficient on basis of the bigger hull side aspect ratio Λ. Since the lateral force resistance coefficient c_{DC} is approximately the same, the hull with the bigger draft has a much more favorable glide ratio c_{CH}.

Fig. 9 Mariner at deeper draft, next page.

Abb. 9

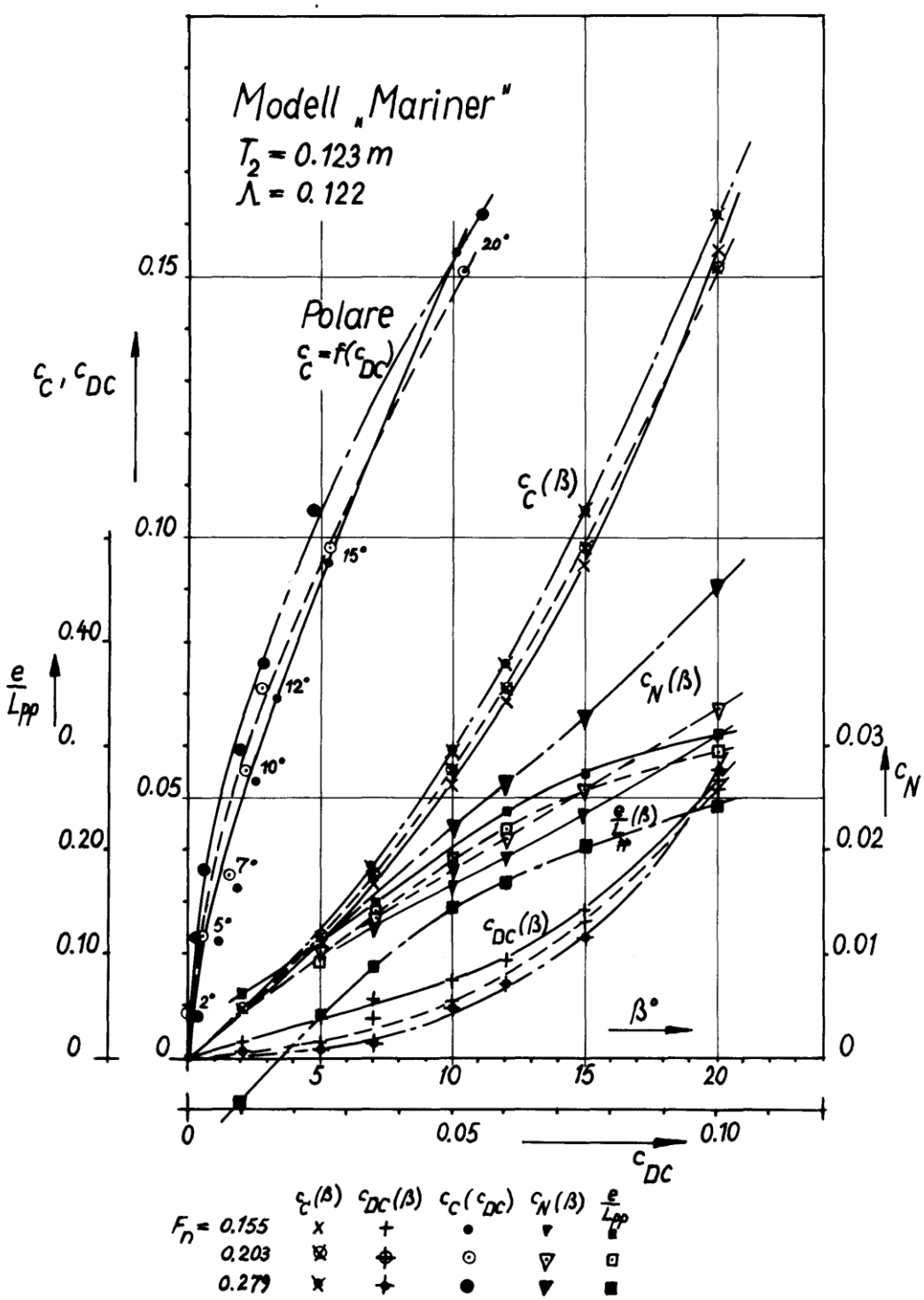

L. A. Ribarov, Translation of B. Wagner's Angled towing tests for a sailing vessel hull with and without bar keel and for the "Mariner" (Schrägschleppversuche für einen Seglerrumpf mit und ohne Balkenkiel und für den "Mariner"), Journal of Merchant Ship Wind Energy, May 2022, www.jmwe.org

Summary

Influence of a bar keel: increase of the lateral force in all investigated angle ranges, such as the lateral force resistance for bigger drift angle. Without keel at small drift angles the center of pressure lies further back.

Influence of the aspect ratios: $\Lambda = 2 \cdot T/L_{pp}$: with increasing Λ, for the same drift angle, the lateral force coefficient c_C increases . Since the influence of Λ on the lateral force resistance coefficient c_{DC} is lower, with growing Λ generally the "hull polar" is more favorable.

Influence of the rudder: increasing rudder angle δ_R, caused an increase of c_C and $c_{DC,}$ and a strong movement of the center of pressure to aft.

Influence of the Froude number: the strongest influence to recognize is the center of pressure location: the pressure point moved forward with rising Froude number. On the other hand, the lateral force resistance coefficient decreased. Lower, and somewhat not as clear is the Froude number influence on the lateral force coefficient.

The qualitative tendencies just described will be further investigated in the next section. On this ground will the test results from known and newly proposed approaches be analyzed.

7. Analysis of the angled towing tests

7.1. Forces on the ship's hull

Underwater ships hulls are bodies with very small aspect ratios. The resulting approaches in Aero- and Hydrodynamics for bodies with small aspect ratios, of which, for example, the ship's rudder is a good example, can only be used conditionally for an underwater ship hull (cf. [5]). Since the contemplated drift angle is small, can one set $\sin \beta = \beta$ and $\cos \beta = 1.00$:

$$c_C = c_1 \cdot \beta + c_2 \cdot \beta^2 \qquad (1)$$ lateral force coefficient

$$c_{DC} = d_1' \cdot \beta^2 + d_2' \cdot \beta^3 \qquad (2)$$ lateral force resistance coefficient

In the approaches will also be used a linear and quadratic term (lateral force coefficient) resp. a quadratic and a cubic term (lateral force resistance coefficient).
Since the method of least squares was run, a balancing calculation for (1) gave a good reproduction of the model test results. The lateral force coefficient can also be represented, for the here presented very small aspect ratios $\Lambda = 0.102$ to 0.155, through a linear and a quadratic term.

A similar analysis of c_{DC} from (2) presented essentially worse results: especially in the range of small b, the lateral force resistance coefficient could not be represented by approach (2), these are significantly above the values obtained from the approach. The approach is also of little suitability of presenting the test results in the range of small drift angle.

Changed approach for c_{DC}

The essential piece of the resistance increase of the angled flow is the "induced resistance":

$$c_{Di} = \frac{c_C^2}{\pi \cdot \Lambda} \quad ; \quad \text{nach (1) ist} \quad c_C^2 = c_1^2 \cdot \beta^2 + 2 c_1 c_2 \cdot \beta^3 + c_2^2 \cdot \beta^4 \ ,$$

,

after that is:

$$c_{Di} = d_1' \cdot \beta^2 + d_2' \cdot \beta^3 + d_3' \cdot \beta^4 \ ;$$

if the 4th degree term is left out, there is agreement with approach (2).

The glide ratio of the forces on the underwater hull is:

$$e_{CH} = \frac{c_{DC}}{c_C} = \frac{c_C}{\pi \cdot \Lambda} \ .$$

On validity from approach (2) had the results c_{CH} to c_C/Λ be constant for all β, and consequently the description of c_{CH} over c_C/Λ had to be a straight line going through the coordinate system origin.

For the specific published model test results ([6] to [10]) of c_{CH} over c_C/Λ for various drift angle β has been assigned in Fig. 11. The registered measurement point that belongs to different models and manifests itself also in wind tunnel results, shows an amazingly low spread.
One cannot use the relation $c_{CH} = f(c_C/\Lambda)$ in the range of approximate small drift angle ($\beta > 2°$) quite well with a straight line that, however, does not go through the zero point, but on the ordinate axis cuts off a certain amount (cf. Fig. 11). In reality, it is a curve, which, for a very small βb, goes to the zero. The measurement accuracy in the area of small drift angles is low, since lateral force resistance coefficient c_{DC} is then very small.
The same can be said also in Fig. 12 where the measurement range of these results is shown where, likewise, is the glide ratio e_{CH} over c_C/Λ applied. Here is under different Froude numbers backwards running scattering of the measurement results bigger than that from model to model. The greater spread in the area of small drift angle (small values c_C/Λ) is explained by the low measurement accuracy in this area. One can for each of the models again approximate the measurement points well with a straight line, which has the gradient k_2 and the absolute value k_1 on the c_{CH} axis cuts off:

$$c_{CH} = k_1 + k_2 \cdot \frac{c_C}{\Lambda} \tag{3}$$

One obtains for the shear force resistance coefficient:

$$c_{DC} = c_{CH} \cdot c_C = k_1 \cdot c_C + k_2 \cdot \frac{c_C^2}{\Lambda} \tag{4}$$

From approach (1), one obtains:

$$c_C = c_1 \cdot \beta + c_2 \cdot \beta^2$$

$$c_C^2 = c_1^2 \cdot \beta^2 + 2c_1 \cdot c_2 \cdot \beta^3 + c_2^2 \cdot \beta^4$$

used in (4):

$$c_{DC} = c_1 \cdot k_1 \cdot \beta + (c_2 \cdot k_1 + \frac{c_1^2 \cdot k_2}{\Lambda}) \cdot \beta^2 + \frac{2c_1 \cdot c_2 \cdot k_2}{\Lambda} \cdot \beta^2 + \frac{c_2^2 \cdot k_1}{\Lambda} \cdot \beta^4 \tag{4a}$$

one obtains the changed approach for c_{DC}:

$$c_{DC} = d_1 \cdot \beta + d_2 \cdot \beta^2 + d_3 \cdot \beta^3 + d_4 \cdot \beta^4 \tag{4b}$$

with the coefficients:

$$d_1 = c_1 \cdot k_1$$

$$d_2 = c_2 \cdot k_1 + \frac{c_1^2 \cdot k_2}{A}$$

$$d_3 = \frac{2c_1 \cdot c_2 \cdot k_2}{A}$$

$$d_4 = \frac{c_2^2 \cdot k_2}{A} \qquad (5)$$

Compared to approach (2), yet another linear term is added by (4b). Furthermore, the 4th degree term is not neglected. The test results were analyzed according to approaches (1) and (3). From the determined factors c_1, c_2, k_1, k_2, the coefficients of the Eq. (4b) can be determined according to (5). This procedure, for systematic reasons of the direct analysis according to (4b), is preferable and can also be better realized graphically. The delivered results are not too scattered. The direct analysis according to (4b) results in greater accuracy of the approximation to the course of the curve, but the obtained coefficients scatter widely according to size and sign and do not reveal any regularity. According to equation (4a), there is adrift angle in the entire range under consideration that makes a good representation of the test results possible. A balancing calculation neglecting the 4th degree term also gives a good approximation of the measurement points, however with strong scattering coefficients. The ones cited above and shown in Fig. 11 were also used for comparison results of other measurements according to the selected approaches (1) and (3). In addition, for the coefficients k_1 and k_2 different mean values were calculated. The identified coefficients are together with the most important model test data of interest summarized in the overview on p. 14.

“page 14” Overview – Results of the adjustment calculations[11]

[11] Added by translator

Modell	Model
Viermastbark mit Kiel	Four-mast barque with keel
ohne Kiel	without keel
Frachter "Mariner" T_1	Freighter "Mariner" T_1
"Mariner" T_2	"Mariner" T_2
Frachter "Serie 60"[9]	Freighter "Series 60" [9]
Forschungssch. "Meteor" [10]	Research ship "Meteor" [10]
Tanker [8]	Tanker [8]
Schoner-brigg [6]	Schooner brig [6]
Strandboot[6]	Coastal boat [6]
Barkasse (HSVA) [7]	Barge (HSVA)

Mittelwerte:		k_1	k_2
alle Messungen	(F_n = 0,155)	0,144 (0,202)	0,185 (0,104)
" "	(F_n = 0,203)	0,054 (0,142)	0,281 (0,159)
" "		0,099 (0,171)	0,233 (0,133)
Messungen nach [6] bis [10]		0,062	0,266
eigene Messungen und Messungen nach [6] bis [10]		0,083	0,248

Averages:
all measurements
" "
" "
measurements from [6] to [10]
own measurements and
measurements from [6] to [10]

Bemerkung:
Klammerwerte ohne $\varepsilon = 2°, 20°$

Remarks:
Values in brackets without $\varepsilon = 2°, 20°$

"page 14"

Übersicht: Ergebnisse der Ausgleichsrechnungen

Modell	$A=\frac{2T}{L_{pp}}$	$\frac{L_{pp}}{B}$	δ	β						c_1	c_2	k_1	k_2	d_1	d_2	d_3	d_4
Viermastbark mit Kiel	0,150	6,71	0,69	0,91	X	X	-	0,155	-	0,227	1,165	0,146	0,172	0,0332	0,2295	0,608	1,559
	0,150	"	"	"	X	X	-	0,203	-	0,211	1,247	0,123	0,163	0,0260	0,2020	0,572	1,688
ohne Kiel	0,142	6,71	0,69	0,91	-	X	-	0,155	-	0,268	0,501	0,143	0,228	0,0383	0,1868	0,431	0,403
	0,142	"	"	"	-	X	-	0,203	-	0,205	0,717	0,170	0,141	0,0349	0,1636	0,292	0,510
Frachter "Mariner" T_1	0,102	6,95	0,60	0,98	-	-	-	0,155	-	0,212	0,494	0,110	0,221	0,0234	0,1520	0,454	0,529
	0,102	"	"	"	-	-	-	0,203	-	0,198	0,507	0,135	0,194	0,0268	0,1433	0,382	0,489
"Mariner" T_2	0,122	6,95	0,62	0,98	-	-	-	0,155	-	0,169	0,775	0,164	0,146	0,0277	0,1611	0,313	0,719
	0,122	"	"	"	-	-	-	0,203	-	0,210	0,626	0,118	0,176	0,0248	0,1374	0,379	0,565
	0,122	"	"	"	-	-	-	0,279	-	0,210	0,727	0,073	0,190	0,0153	0,1217	0,476	0,822
Frachter "Serie 60"[9]	0,107	7,50	0,60	0,98	-	-	-0,20+0,24		-	0,213	0,976	0,032	0,357	0,0067	0,1815	1,384	3,179
Forschungssch. "Meteor" [10]	0,138	5,39	0,54	0,88	-	X	-	$-1{,}76\cdot10^6$		0,173	0,772	0,063	0,278	0,0108	0,1097	0,546	1,217
Tanker [8]	0,1057	6,91	0,75	0,99	-	-	-	0,160	-	0,244	0,880	0,089	0,214	0,0216	0,1980	0,867	1,567
Schoner-brigg [6]	0,248	4,15	0,57	-	X	X	-	$-1{,}01\cdot10^6$		0,284	1,322	0,073	0,244	0,0206	0,1754	0,740	1,722
Strandboot[6]	0,186	3,72	-	-	X	X	X	$-1{,}01\cdot10^6$		0,287	0,995	0,014	0,399	0,0039	0,1908	1,226	2,122
Barkasse (HSVA) [7]	0,161	4,61	0,38	-	X	X	X	0,179	-	0,239	1,840	0,048	0,290	0,0115	0,1913	1,583	6,085

Mittelwerte:	k_1	k_2
alle Messungen (F_n = 0,155)	0,144 (0,202)	0,185 (0,104)
" " (F_n = 0,203)	0,054 (0,142)	0,281 (0,159)
" "	0,099 (0,171)	0,233 (0,133)
Messungen nach [6] bis [10]	0,062	0,266
eigene Messungen und Messungen nach [6] bis [10]	0,083	0,248

Bemerkung:
Klammerwerte ohne $\varepsilon = 2^0, 20^0$

1. Analysis of the lateral force coefficients (from approach (1)):

$$c_C = c_1 \cdot \beta + c_2 \cdot \beta^2$$

Splitting the shear (lateral) force coefficients into linear ("waterline-") part and a square ("frame") part is possible with good accuracy. The coefficients of both parts depend mainly on the following variables: aspect ratio Λ, length-to-width ratio, L_{pp}/B, hull and main frame (midship) shape (β, dead rise, bar keel, bilge keels, keel rake), experimental method ("medium"), Froude number.

The coefficient of the linear part c_1 has an increasing tendency with A which can be explained quite well with the theoretically derived value represented as $c_1 = \pi/2 \cdot \Lambda$ (cf. [4]). The influence of L/B and the main frame shape seems to be secondary. Of greater contrast is the Froude number influence on c_1. In general, c_1 will get smaller with increasing Froude number.

The coefficient of the quadratic term c_2 is also bigger with Λ. Here, however, the influence of the main shape is greater: e.g. by attaching a bar keel to the sailing vessel hull, c_2 approximately doubles. The approximation formula given in [5]

$$c_2 \approx c_{DC\infty} \cdot (1 + 0{,}82 \cdot /\Lambda)$$

results in coefficients that are too high throughout the Λ range, even if for the transverse resistance command $c_{DC\infty} = 1.00$ is set (at $\Lambda = 0$ applies $c_{DC\infty} = 1.00$ (2.00) for round (sharp-edged bodies). With increasing Froude number c_2 became bigger, while c_1 became smaller. This means that for bigger Froude numbers at small drift angles initially smaller shear force coefficients occur, with medium ones up to large drift angles, however, this difference disappears or becomes smaller, due to the larger factor of the quadratic term.

2. Analysis of the shear (lateral) force resistance coefficient c_{DC}

This analysis was carried out expediently (see above!) by determining the factors k_1 and k_2 according to approach (3). The coefficients d_1 through d_4 in the equation (4b) then were determined from (5). The values k_1 and k_2 obtained by fitting calculation are included in the overview on p. 14. As mentioned, the influence of the Froude number on k_1 and k_2 is bigger than the dependency on ship type. If one does not use the measurement results for the adjustment calculation for very large drift angles ($\beta = 20°$) or very small drift angles ($\beta = 2°$, low measurement accuracy), one also gets deviating coefficients k_1 and k_2. As it is seen from the given overview of the mean values for k1 and k_2, k_1 is smaller with increasing Froude number, while k_2 becomes larger. If one does not take into account the readings for $\beta = 2°$ and 20° in the evaluation, the coefficients k_1 increase while the ones for k_2 get smaller (values in brackets in the overview).

When calculating c_{DC}, it is not possible to use the coefficients d_1 through d_4 from a suitable test model, it is always advisable to first make assumptions for the values k_1 and k_2, e.g. according to the specified overall values taking into account the Froude number. The factors d_1 through d_4 can then be calculated with good accuracy with the help from c_1, c_2, k_1, and k_2 from (5). In equation (4b) the 4th degree term cannot be neglected since the coefficient d_4 is relatively large (see overview page 14). On the coefficients of the comparatively given results other attempt ([6] to [10]) should be noted that partly only the angular range up to $\beta = 10°$ is recorded which resulted in relatively small values for k_1 and larger values for k_2.

7.2 Influence of the rudder angle δ_R

The experiments were carried out without propeller. The rudder flow speed, which greatly affects rudder force, depends on the flow of the ship's hull. This in turn, in place of the rudder, depends on the drift angle. One can set for the rudder inflow speed:

$$V_R = V(w_1 + w_2 \cdot \beta) \qquad (6)$$

The influence of the deflection effect of the ship's hull on the effective flow angle of the rudder is in the tests with $\delta_R = 0°$ already included, so that additional resistance and additional transverse force result in rudder position that can be specified as a function of the rudder angle δ_R. For simplification, for the rise in the lateral force with δ_R a linear and correspondingly a quadratic approach for the resistance is chosen:

$c_{CR}' = a_1 \cdot \delta_R$ Rudder lateral force coefficient

$c_{DR}' = a_2 \cdot \delta_R^2$ Rudder resistance coefficient

For rudder lateral force and rudder resistance, the result is then:

$$C_R = c_{CR}' \cdot \frac{\rho}{2} V_R^2 \cdot L_{pp} \cdot T = a_1 \cdot \delta_R \cdot \frac{\rho}{2} V^2 (w_1^2 + 2 w_1 w_2 \cdot \beta + w_2^2 \cdot \beta^2) L_{pp} T \qquad (7)$$

$$D_R = a_2 \cdot \delta_R^2 \cdot \frac{\rho}{2} V^2 (w_1^2 + 2 w_1 w_2 \cdot \beta + w_2^2 \cdot \beta^2) \cdot L_{pp} \cdot T \qquad (8)$$

Additional transverse force and additional resistance through the rudder in relation to "lateral surface" $L_{pp} \cdot T$ and ship speed V becomes:

$$c_{CR} = c_{R1} \cdot \delta_R + c_{R2} \cdot \delta_R \cdot \beta + c_{R3} \cdot \delta_R \cdot \beta^2 \qquad (9)$$

$$c_{DR} = d_{R1} \cdot \delta_R^2 + d_{R2} \cdot \delta_R^2 \cdot \beta + d_{R3} \cdot \delta_R^2 \cdot \beta^2 \qquad (10)$$

Angled towing tests with different rudder positions were carried out for the sailing vessel hull with bar keel. With the measurement results, a compensation calculation was carried out for c_{CR} and c_{DR}, with and without the β^2-terms. It resulted in the following overview of compiled coefficients:

F_n	c_{R1}	c_{R2}	c_{R3}	d_{R1}	d_{R2}	d_{R3}		
0,155	0,0346	-0,135	0,720	0,0242	-0,205	1,691	mit β^2 - Gliedern	with β^2 – terms
0,203	0,0336	0,096	-0,033	0,0229	-0,200	2,412		
0,155	0,0277	0,0527	-	0,0079	0,237	-	ohne β^2 - Glieder	without β^2 – terms
0,203	0,0339	0,0873	-	-0,0003	0,430	-		

While showing the additional lateral force coefficients Δc_C of the term $c_{R3} \cdot \delta_R \cdot \beta^2$ can be omitted, it is for better representation of the additional drag coefficient c_{DR}, that the term $d_{R3} \cdot \delta_R^2 \cdot \beta^2$ is required.

8. Conclusion

The present report contains the results from angled towing tests with 2-m models of a sailing ship (with and without bar keel) and the “Mariner” (in 2 drafts). Investigated and explained are the influences from bar keel, body shape planform, aspect ratio, rudder position and Froude number on the magnitude of the force coefficients and the yaw moments of the underwater hull.

A bar keel and an increase in the aspect ratio have an effect of increasing the lateral force. The influence on the lateral force resistance is smaller, so that these measurement result in more favorable glide ratios (lateral force resistance/ lateral force).

A rudder angle causes an increase in lateral force and lateral force resistance, but above all, the center of pressure shifts backwards. The influence of the Froude number is also great: the lateral force resistance coefficient decreases with increasing Froude number, while the center of pressure shifts forward.

The analysis of the test results by the method of least squares showed that the lateral force coefficients are well represented through a linear and a quadratic term depending on the value of the drift angle.

In contrast, the representation of the lateral force resistance through a square and a cubic term was unsatisfactory for smaller drift angles. A significant improvement was achieved by adding a linear term. For systematic reasons it is recommended that analysis of a plot of the glide ratio of the forces on the surface ship (above the waterline) over the associated values of c_C/Λ be completed. It turns out then there is a payoff when showing the lateral force resistance also a 4th degree term.

9. Symbols overview

L_{pp} ..... Length between perpendiculars

B ..... Width

T ..... Draft

∇ ..... Volume displacement

δ ..... Block coefficient

A_L ..... Lateral surface of the underwater hull

$\Lambda = 2 \cdot T/L_{pp}$ ..... Aspect ratio of the underwater hull

V, V_R ..... Inflow speeds of the ship or ships' rudder

F_n ..... Froude Number

R_n ..... Reynolds Number

β ..... Drift angle

δ_R ..... Ruder position angle

F_T ..... Force on underwater hull

C ..... Component of force perpendicular to the flow direction ("lateral force")

D ..... Component of force in the flow direction ("resistance")

D_0 ..... Resistance of forward motion without drift

D_C ..... Resistance increase at oblique flow ("lateral force resistance")

D_R ..... Resistance increase at rudder position δ_R

D_i ..... Induced resistance

X ..... Component of force in the ship's longitudinal direction ("longitudinal direction")

Y ..... Component of force perpendicular to the ship's longitudinal direction ("side force")

$c_{FT}, c_C, c_D, c_{DO},$

c_{DC}, c_{DR}, c_X, c_Y .. Dimensionless coefficients of the force components and drag components related to the dynamic pressure and the lateral area

N ..... Yaw moment in terms of $L_{pp}/2$

c_N ..... Yaw moment coefficient based on dynamic pressure q, lateral surface $A_L = L_{pp} \cdot T$ and length L_{pp}

$q = \frac{\rho}{2} \cdot v^2$ ..... Dynamic pressure of the flow velocity (ρ….. density of water)

x_F ..... Point position of the lateral force of the hull in relation to the zero point moment ($L_{pp}/2$)

$\bullet$ ..... Point position of the lateral force of the hull behind the forward perpendicular

$c_{CH} = D_C/C$ ..... Glide ratio of the forces on the underwater hull

c_1, c_2 ..... Coefficients of Terms 1, and 2. Degrees for the shear force coefficient

$d_1 - d_4$ ..... Coefficients of Terms 1, through 4. Degrees for the shear resistance coefficient

k_1, k_2 ..... Coefficients representing the glide ratio of the forces on the underwater hull as a function of c_C/Λ

w_1, w_2 ..... Coefficients representing wake influence of the rudder flow velocity V_R

$c_{R1} - c_{R3}$ ..... Coefficients representing c_{CR} as a function of δ_R and β

$d_{R1} - d_{R3}$ ..... Coefficients representing c_{DR} as a function of δ_R and β

10. References

[1] Wagner, B.: "Fahrtgeschwindigkeitsberechnung für Segelschiffe", IfS-Bericht Nr. 132 (1967), Jahrb. der STG 61 (1967).

[2] Wagner, B.: "Windkräfte an Überwasserschiffen", Jahrb. STG 61 (1967).

[3] Johow-Foerster: "Hilfsbuch für den Schiffbau", 4. Auflage, Verlag von Julius Springer, Bd. II, Tafel VI.

[4] Russo und Sullivang: "Design of the Mariner-Type Ship", SNAME

[5] Thieme, H.: "Über strömungstechnische Grundlagen zur Bestimmung von Steuereigenschaften", Schiff und Hafen 6 (1954), S. 510.

[6] Frey, K.: "Theorie des Segelns mit Abtriftberücksichtigung", Jahrb. der STG (1933), S. 228.

[7] Thieme, H.: "Schrägschleppversuche mit einem geraden und einem gekrümmten Barkassenmodell", Schiff und Hafen, 8 (1956), Heft 4.

[8] Bülow, H.: "Hydrodynamische Untersuchungen zur Bestimmung von Stabilitätskriterien stationär bewegter Körper", IfS-Bericht Nr. 108

[9] Eda, H. und Crane, C.L.: "Steering Characteristics of Ships in Calm Water and Waves", Transact. SNAME (1965).

[10] Wagner, B.: "Windkanalversuche mit dem Modell des Forschungsschiffes METEOR", IfS-Bericht Nr. 153 (1966).

APPENDIX

Angled towing test results for the sailing vessel hull with- and without heeling

The test results were performed in the towing tank of the Engineering School of Hamburg am Berliner Tor with heeling $\varphi = 0°$ and 10°.

Test data:

Tank measurements:	Length	40 m
	Width	6.5 m
	Depth	2 m
Towing speeds:	0.38 to 1.27 m/s	
Froude numbers F_n:	0.087 to 0.267	
Measurement method:	Pendulum wire with pre-weights	
Turbulence generator:	Perlon wire on frame 9 ½	

Model dimensions: cf. Section 3 where the full model with bar keel was examined.

The test results are contained in Table 7 and presented in Fig. 13 in dimensionless form. It shows that the heeling angle of $\varphi = 10°$ used here is only of minor influence on the resistance. For a better comparison with the drag coefficients in the Tables 1 to 6 are the drag coefficients - different from the usual normalization - related to the area $L_{pp} \cdot T$. The influence of the turbulence generators on the resistance is corrected.

Table 1.1 and 1.2 (cf. Fig. 4)
(editor's's note: it appears that here the Greek letter ε represents the drift or leeway angle in degrees. In the text it is referred to as β.)

Table 1.1: Four-mast barque with keel
$\Lambda = \frac{2 \cdot T}{L_{pp}} = 0.150$; $\delta_R = 0°$; $F_n = 0.155$

Tab. 1.1 und 1.2 (vgl. Abb. 4)

Tab. 1.1: Viermastbark mit Kiel

$\Lambda = \frac{2 \cdot T}{L_{pp}} = 0,150$; $\delta_R = 0^o$; $F_n = 0,155$

ε	c_C	c_D	c_{DC}	c_N	e/L_{pp}
0	0,0000	0,01667	0,00000	0,00000	-
2	0,0118	0,01830	0,00163	0,00428	0,154
5	0,0301	0,02288	0,00621	0,01001	0,187
7	0,0458	0,02549	0,00882	0,01318	0,228
10	0,0745	0,03333	0,01667	0,01667	0,289
12	0,0974	0,04216	0,02549	0,01846	0,323
15	0,1386	0,06111	0,04444	0,02056	0,363
20	0,2222	0,10359	0,08693	0,02304	0,406

Table 1.2: Four-mast barque with keel

$\Lambda = \frac{2 \cdot T}{L_{pp}} = 0.150$; $\delta_R = 0°$; $F_n = 0.203$

Tab. 1.2: Viermastbark mit Kiel

$\Lambda = \frac{2 \cdot T}{L_{pp}} = 0{,}150$; $\delta_R = 0^o$; $F_n = 0{,}203$

ε	c_C	c_D	c_{DC}	c_N	e/L_{pp}
0	0,0000	0,01699	0,00000	0,00000	-
2	0,0098	0,01830	0,00131	0,00412	0,105
5	0,0288	0,02157	0,00458	0,01032	0,162
7	0,0444	0,02484	0,00784	0,01363	0,211
10	0,0739	0,03105	0,01405	0,01724	0,279
12	0,0980	0,03987	0,02288	0,01882	0,319
15	0,1418	0,05588	0,03889	0,02099	0,361
20	0,2255	0,10065	0,08366	0,02567	0,396

Table 2: (cf. Fig. 5)

Table 2: Four-mast barque with keel

$\Lambda = \frac{2 \cdot T}{L_{pp}} = 0.150$; $\delta_R = 10°$; $F_n = 0.155$

Tab. 2 (vgl. Abb. 5)

Tab. 2: Viermastbark mit Kiel

$\Lambda = \frac{2 \cdot T}{L_{pp}} = 0{,}150$; $\delta_R = 10^o$; $F_n = 0{,}155$

ε	c_C	c_D	c_{DC}	c_N	e/L_{pp}
0	0,0072	0,01699	0,00000	-0,00185	0,757
2	0,0137	0,01961	0,00261	0,00166	0,385
5	0,0294	0,02288	0,00588	0,00678	0,283
7	0,0458	0,02614	0,00915	0,00984	0,297
10	0,0765	0,03725	0,02026	0,01300	0,341
12	0,1020	0,04510	0,02810	0,01434	0,369
15	0,1451	0,06340	0,04641	0,01548	0,401

Table 3.1 and 3.2: (cf. Fig. 5 and 6)

Table 3.1: Four-mast barque with keel

$\Lambda = \frac{2 \cdot T}{L_{pp}} = 0.150$; $\delta_R = 20°$; $F_n = 0.150$

Tab. 3.1 und 3.2 (vgl. Abb. 5 und 6

Tab. 3.1: Viermastbark mit Kiel

$\Lambda = \frac{2 \cdot T}{L_{pp}} = 0{,}150$; $\delta_R = 20^o$; $F_n = 0{,}155$

ε	c_C	c_D	c_{DC}	c_N	e/L_{pp}
0	0,0124	0,01961	0,00000	-0,00413	0,833
2	0,0203	0,02222	0,00261	-0,00046	0,522
5	0,0386	0,02484	0,00523	0,00379	0,407
7	0,0569	0,02876	0,00915	0,00607	0,399
10	0,0902	0,03922	0,01961	0,00877	0,408
12	0,1157	0,04902	0,02941	0,00984	0,420
15	0,1562	0,06993	0,05033	0,01036	0,439

Table 3.2: Four-mast barque with keel

$\Lambda = \frac{2 \cdot T}{L_{pp}} = 0.150$; $\delta_R = 20°$; $F_n = 0.203$

Tab. 3.2: Viermastbark mit Kiel

$\Lambda = \frac{2 \cdot T}{L_{pp}} = 0{,}150$; $\delta_R = 20^o$; $F_n = 0{,}203$

ε	c_C	c_D	c_{DC}	c_N	e/L_{pp}
0	0,0118	0,01961	0,00000	-0,00306	0,760
2	0,0209	0,02222	0,00261	0,00028	0,487
5	0,0425	0,02484	0,00523	0,00503	0,387
7	0,0595	0,02876	0,00915	0,00739	0,382
10	0,0922	0,03856	0,01895	0,00996	0,398
12	0,1176	0,05098	0,03137	0,01115	0,411
15	0,1601	0,07190	0,05229	0,01191	0,431

Table 4.1 and 4.2: (cf. Fig. 7)

Table 4.1: Four-mast barque without keel

$\Lambda = \frac{2 \cdot T}{L_{pp}} = 0.142$; $\delta_R = 0°$; $F_n = 0.155$

Tab. 4.1 und 4.2 (vgl. Abb. 7)

Tab. 4.1: Viermastbark ohne Kiel

$\Lambda = \frac{2 \cdot T}{L_{pp}} = 0{,}142$; $\delta_R = 0^o$; $F_n = 0{,}155$

ε	c_C	c_D	c_{DC}	c_N	e/L_{pp}
0	0,0000	0,01761	0,00000	0,00000	-
2	0,0131	0,01795	0,00035	0,00329	0,261
5	0,0290	0,02624	0,00863	0,00802	0,243
7	0,0400	0,02831	0,01070	0,01062	0,254
10	0,0608	0,03279	0,01519	0,01363	0,292
12	0,0773	0,03659	0,01899	0,01544	0,314
15	0,1043	0,04902	0,03141	0,01814	0,340
20	0,1553	0,07664	0,05903	0,02198	0,372

Table 4.2: Four-mast barque without keel

$\Lambda = \frac{2 \cdot T}{L_{pp}} = 0.142$; $\delta_R = 0°$; $F_n = 0.203$

Tab. 4.2: Viermastbark ohne Kiel

$\Lambda = \frac{2 \cdot T}{L_{pp}} = 0,142$; $\delta_R = 0^o$; $F_n = 0,203$

ε	c_C	c_D	c_{DC}	c_N	e/L_{pp}
0	0,0000	0,01795	0,00000	0,00000	-
2	0,0097	0,01381	-0,00414	0,00262	0,242
5	0,0242	0,02209	0,00414	0,00805	0,190
7	0,0352	0,02624	0,00829	0,01099	0,212
10	0,0573	0,03107	0,01312	0,01424	0,270
12	0,0746	0,03521	0,01726	0,01648	0,295
15	0,1029	0,04626	0,02831	0,02090	0,312
20	0,1574	0,07249	0,05454	0,02726	0,342

Table 5.1 and 5.2: (cf. Fig. 8)

Table 5.1: "Mariner", $T_1 = 0.103$ m

$\Lambda = \frac{2 \cdot T}{L_{pp}} = 0.102$; $\delta_R = 0°$; $F_n = 0.155$

Tab. 5.1 und 5.2 (vgl. Abb. 8)

Tab. 5.1: "Mariner", $T_1 = 0,103$ m

$\Lambda = \frac{2 \cdot T}{L_{pp}} = 0,102$; $\delta_R = 0^o$; $F_n = 0,155$

ε	c_C	c_D	c_{DC}	c_N	e/L_{pp}
0	0,0000	0,01892	0,00000	0,00000	
2	0,0090	0,01987	0,00095	0,00329	0,160
5	0,0232	0,02318	0,00426	0,00782	0,189
7	0,0331	0,02413	0,00520	0,01045	0,208
10	0,0511	0,03122	0,01230	0,01402	0,248
12	0,0662	0,03690	0,01798	0,01647	0,273
15	0,0894	0,04636	0,02744	0,02028	0,294
20	0,1344	0,07096	0,05204	0,02785	0,315

Table 5.2: “Mariner”, T_1 = 0.103 m
$\Lambda = \frac{2 \cdot T}{L_{pp}}$ = 0.102; δ_R = 0°; F_n = 0.203

Tab. 5.2: "Mariner", T_1 = 0,103 m

$\Lambda = \frac{2 \cdot T}{L_{pp}}$ = 0,102 ; δ_R = 0° ; F_n = 0,203

ε	c_C	c_D	c_{DC}	c_N	e/L_{pp}
0	0,0000	0,01892	0,00000	0,00000	-
2	0,0090	0,01987	0,00095	0,00364	0,124
5	0,0222	0,02318	0,00426	0,00829	0,157
7	0,0317	0,02460	0,00568	0,01114	0,177
10	0,0492	0,03028	0,01135	0,01502	0,220
12	0,0634	0,03501	0,01608	0,01764	0,245
15	0,0870	0,04542	0,02649	0,02152	0,275
20	0,1325	0,08894	0,07002	0,03135	0,298

Table 6.1 to 6.3: (cf. Fig. 9)

Table 6.1: “Mariner”, T_2 = 0.123 m
$\Lambda = \frac{2 \cdot T}{L_{pp}}$ = 0.122; δ_R = 0°; F_n = 0.155

Tab. 6.1 bis 6.3 (vgl. Abb. 9)

Tab. 6.1: "Mariner", T_2 = 0,123 m

$\Lambda = \frac{2 \cdot T}{L_{pp}}$ = 0,122 ; δ_R = 0° ; F_n = 0,155

ε	c_C	c_D	c_{DC}	c_N	e/L_{pp}
0	0,0000	0,01762	0,00000	0,00000	-
2	0,0095	0,01793	0,00031	0,00443	0,061
5	0,0221	0,02355	0,00593	0,00960	0,101
7	0,0328	0,02670	0,00908	0,01262	0,148
10	0,0529	0,03035	0,01273	0,01665	0,190
12	0,0687	0,03440	0,01678	0,01940	0,239
15	0,0948	0,04425	0,02663	0,02360	0,271
20	0,1548	0,06800	0,05038	0,03150	0,313

Table 6.2: “Mariner”, T_2 = 0.123 m
$\Lambda = \frac{2 \cdot T}{L_{pp}}$ = 0.122; δ_R = 0°; F_n = 0.203

Tab. 6.2: "Mariner", T_2 = 0,123 m

$\Lambda = \frac{2 \cdot T}{L_{pp}}$ = 0,122 ; δ_R = 0° ; F_n = 0,203

ε	c_C	c_D	c_{DC}	c_N	e/L_{pp}
0	0,0000	0,01762	0,00000	-0,00000	-
2	0,0087	0,01738	-0,00024	0,00428	0,039
5	0,0233	0,02054	0,00292	0,01016	0,094
7	0,0352	0,02528	0,00766	0,01359	0,142
10	0,0553	0,02804	0,01043	0,01821	0,193
12	0,0711	0,03160	0,01398	0,02120	0,221
15	0,0980	0,04424	0,02662	0,02581	0,257
20	0,1509	0,06952	0,05190	0,03346	0,298

Table 6.3: "Mariner", T_2 = 0.123 m

$\Lambda = \frac{2 \cdot T}{L_{pp}}$ = 0.122; δ_R = 0°; F_n = 0.279

Tab. 6.3: "Mariner", T_2 = 0,123 m

$\Lambda = \frac{2 \cdot T}{L_{pp}}$ = 0,122 ; δ_R = 0° ; F_n = 0,279

ε	c_C	c_D	c_{DC}	c_N	e/L_{pp}
0	0,0000	0,01927	0,00000	0,00001	-
2	0,0083	0,02054	0,00126	0,00491	-0,046
5	0,0237	0,02133	0,00205	0,01171	0,040
7	0,0363	0,02212	0,00284	0,01593	0,089
10	0,0592	0,02923	0,00995	0,02231	0,148
12	0,0758	0,03357	0,01430	0,02655	0,173
15	0,1051	0,04266	0,02338	0,03283	0,208
20	0,1619	0,07505	0,05577	0,04557	0,244

Fig. 10 Definition sketch for force components and yaw moment

Abb. 10

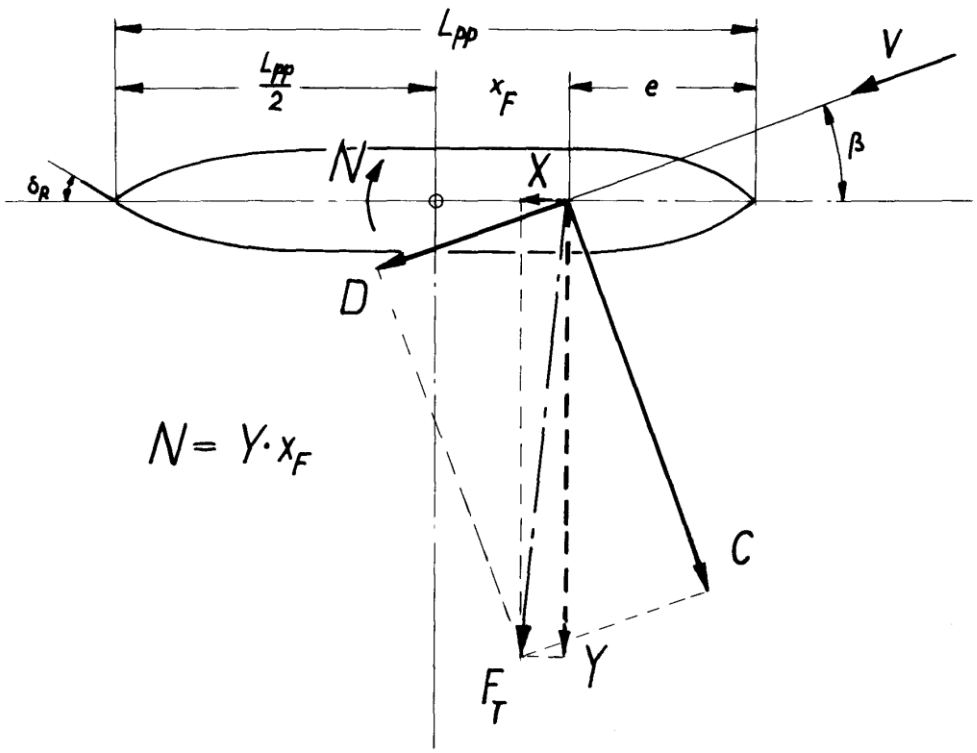

Definitionsskizze für Kraftkomponenten und Giermoment

Fig. 11 Representations $\varepsilon_{CH} = f\left(\frac{c_C}{\Lambda}\right)$

Schooner brig [6]
Coastal boat [6]
Barge [7]
Tanker [8]
Cargo ship "Series 60" [9]
"Meteor" [10]

Abb. 11

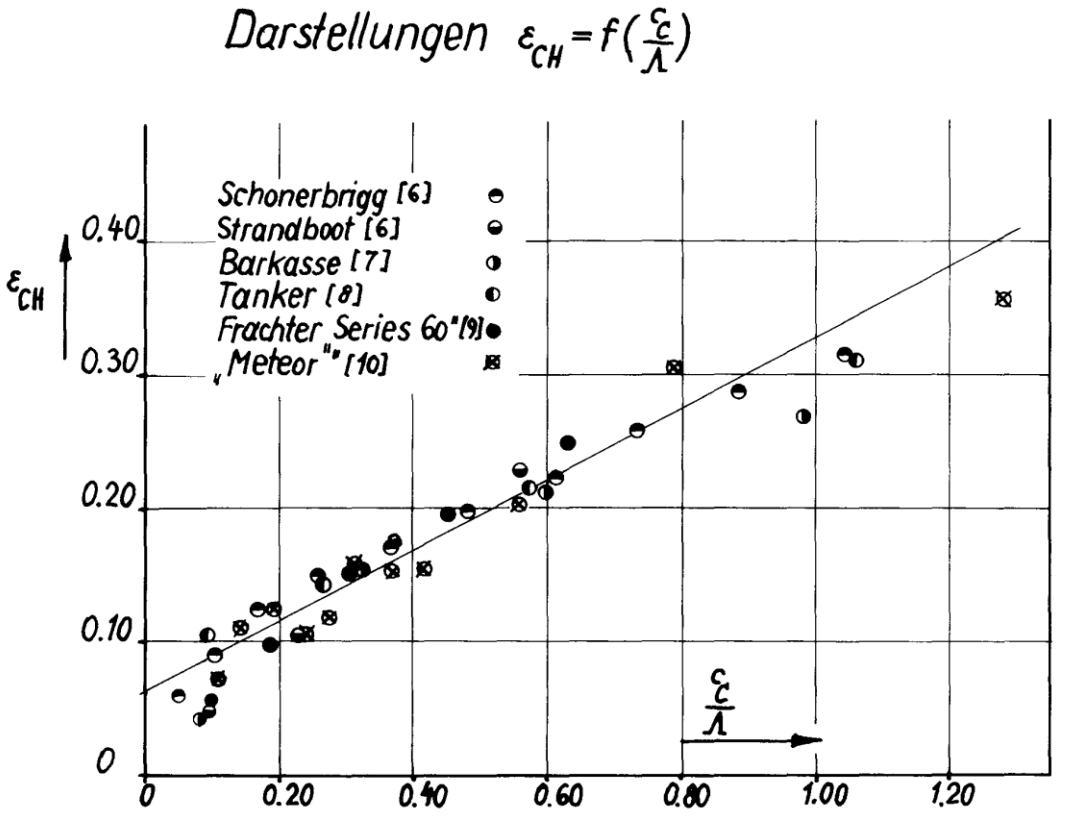

Fig. 12 Representations $\varepsilon_{CH} = f\left(\frac{c_C}{\Lambda}\right)$

Sailing ship with bar keel
Sailing ship without bar keel
"Mariner" T_1
"Mariner" T_2

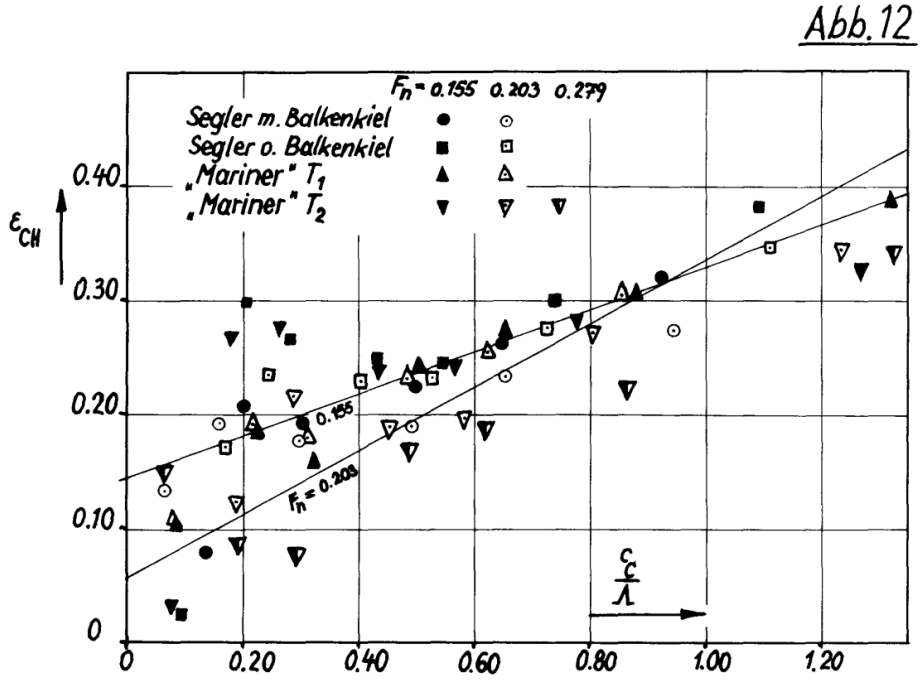

Fig. 13 Influence of heeling on the resistance of straight ahead movement

$$c_{D0} = \frac{D_0}{\frac{\rho}{2} \cdot V^2 \cdot L_{pp} \cdot T}$$

Model-resistance
Sailing ship-hull

Abb. 13

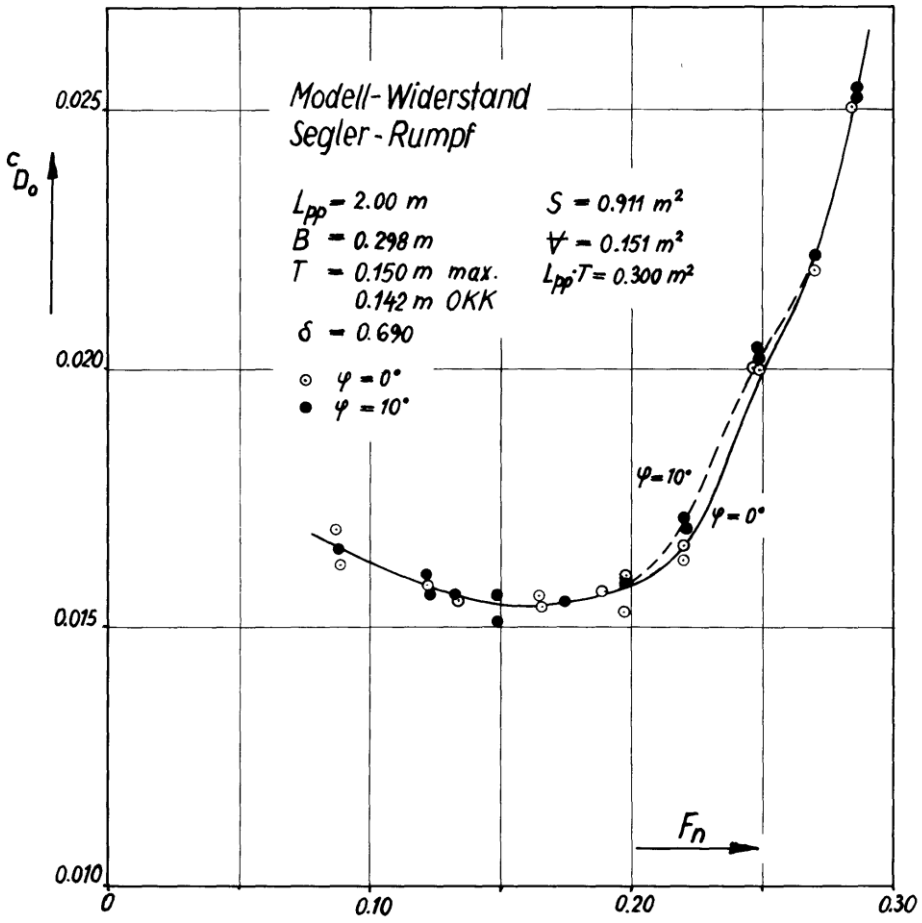

Einfluß der Krängung auf den Widerstand
bei Geradeausfahrt

$$c_{D0} = \frac{D_0}{\frac{\rho}{2} \cdot V^2 \cdot L_{pp} \cdot T}$$